ARMY RESEARCH LABORATORY

Bimolecular Recombination Kinetics of an Exciton–Trion Gas

by Frank Crowne and A Glen Birdwell

ARL-TR-7355 July 2015

Approved for public release; distribution unlimited.

NOTICES

Disclaimers

The findings in this report are not to be construed as an official Department of the Army position unless so designated by other authorized documents.

Citation of manufacturer's or trade names does not constitute an official endorsement or approval of the use thereof.

Destroy this report when it is no longer needed. Do not return it to the originator.

Army Research Laboratory
Adelphi, MD 20783-1138

ARL-TR-7355 **July 2015**

Bimolecular Recombination Kinetics of an Exciton–Trion Gas

Frank Crowne and A Glen Birdwell
Sensors and Electron Devices Directorate, ARL

Approved for public release; distribution unlimited.

REPORT DOCUMENTATION PAGE

Form Approved
OMB No. 0704-0188

Public reporting burden for this collection of information is estimated to average 1 hour per response, including the time for reviewing instructions, searching existing data sources, gathering and maintaining the data needed, and completing and reviewing the collection information. Send comments regarding this burden estimate or any other aspect of this collection of information, including suggestions for reducing the burden, to Department of Defense, Washington Headquarters Services, Directorate for Information Operations and Reports (0704-0188), 1215 Jefferson Davis Highway, Suite 1204, Arlington, VA 22202-4302. Respondents should be aware that notwithstanding any other provision of law, no person shall be subject to any penalty for failing to comply with a collection of information if it does not display a currently valid OMB control number.
PLEASE DO NOT RETURN YOUR FORM TO THE ABOVE ADDRESS.

1. REPORT DATE *(DD-MM-YYYY)*	2. REPORT TYPE	3. DATES COVERED (From - To)
July 2015	Final	09/2013–09/2014

4. TITLE AND SUBTITLE
Bimolecular Recombination Kinetics of an Exciton–Trion Gas

5a. CONTRACT NUMBER

5b. GRANT NUMBER

5c. PROGRAM ELEMENT NUMBER

6. AUTHOR(S)
Frank Crowne and A Glen Birdwell

5d. PROJECT NUMBER

5e. TASK NUMBER

5f. WORK UNIT NUMBER

7. PERFORMING ORGANIZATION NAME(S) AND ADDRESS(ES)
US Army Research Laboratory
ATTN: RDRL-SER-E
2800 Powder Mill Road
Adelphi, MD 20783-1138

8. PERFORMING ORGANIZATION REPORT NUMBER
ARL-TR-7355

9. SPONSORING/MONITORING AGENCY NAME(S) AND ADDRESS(ES)
Joe Qiu
US Army Research Office
PO Box 12211, Research Triangle Park, NC 27709-2211

10. SPONSOR/MONITOR'S ACRONYM(S)

11. SPONSOR/MONITOR'S REPORT NUMBER(S)

12. DISTRIBUTION/AVAILABILITY STATEMENT
Approved for public release; distribution unlimited.

13. SUPPLEMENTARY NOTES

14. ABSTRACT

This report discusses the use of rate equations to describe kinetic processes in highly photoexcited semiconductors. In this description, the pairs of electrons and holes generated by photons from the laser illumination form a multicomponent plasma whose time evolution is governed by gas dynamics and recombination processes, leading to a variety of secondary components such as neutral excitons and so-called trions, which consist of exciton–electron and exciton–hole bound states. The recombination is modeled as bimolecular for all carrier species, allowing the system of rate equations to be simulated numerically.

15. SUBJECT TERMS
excitons, trions, bimolecular recombination, 2-D

16. SECURITY CLASSIFICATION OF:			17. LIMITATION OF ABSTRACT	18. NUMBER OF PAGES	19a. NAME OF RESPONSIBLE PERSON
a. REPORT	b. ABSTRACT	c. THIS PAGE			Frank Crowne
Unclassified	Unclassified	Unclassified	UU	26	19b. TELEPHONE NUMBER (*Include area code*) 301-394-5759

Standard Form 298 (Rev. 8/98)
Prescribed by ANSI Std. Z39.18

Contents

List of Figures

List of Tables

1. Introduction

The technique of photoluminescence (PL) is customarily used to investigate band structure and other single-particle states of a solid by monitoring electronic transitions induced by incident high-energy photons.[1] However, PL excitation also leaves the solid in a high-energy state (here referred to as a solid-state plasma (SSP) characterized by various many-body correlated subsystems. Among these are

- the electron and hole gases, consisting of free electrons (denoted by *e*) and free holes (denoted by *h*)
- the exciton gas, consisting of bound electron-hole pairs (denoted by *eh*)
- the biexciton gas, consisting of pseudo-hydrogen molecules (denoted by *eehh*)
- the trion gases, consisting of bound carrier triplets (*eeh* denotes an *e*–trion, *ehh* an *h*–trion)
- electron-hole droplets

Because all of these species are present at once when a solid is under PL excitation, their mutual interactions and carrier kinetics are important in interpreting experimental data.

In 3-dimensional (3-D) systems (i.e., bulk solids) SSPs are usually observed only at low temperatures, since the constituent carriers consist of weakly bound "molecules" made up of the PL-excited free electrons and holes. However, these entities have much larger binding energies in 2-dimensional (2-D) systems, notably in the transition-metal dichalcogenides (TMDs) such as molybdenum disulfide (MoS_2) and tungsten diselenide. High-order correlated states (excitons, trions, biexcitons, triexcitons, etc.) have been observed experimentally in PL-excited carrier gases primarily in pseudo-2-D systems such as quantum wells[2]; however, the recent observation of trions in MoS_2 by Mak et al.[3] has generated renewed interest in these truly 2-D systems, and in particular has motivated the writing of this report.

2. Formalism

It is instructive to examine SSPs using lowest-order kinetic theory, which is formulated in terms of systems of spatially uniform rate equations.[4] A system of this kind usually consists of N nonlinear differential equations, one for each of the N distinct carrier species, with N first-order time dependent densities:

$$\frac{\partial}{\partial t} f_i(t) = G_i - \Re_i\left(f_1, f_2, f_3, \ldots, f_N\right) \;,\; i = 1,2,3,\ldots,N \tag{1}$$

where G_i are source terms originating from the incident PL photon flux and $\Re_i$ denotes the recombination rate for the *i* – th species. In this context, "bimolecular" recombination implies that the $\Re_i$ consist of sums of quadratic terms, each of which is the product of 2 carrier densities. Positive terms in $\Re_i$ tend to increase the density of carrier *i*, negative terms to decrease it. Currently, the most interesting PL-induced systems are the 2-D monolayers, in which recombination dynamics can be complicated; for simplicity's sake the modeling described in this technical report is based on simple (i.e., "pure") bimolecular recombination laws, which can be rigorously justified for 3-D systems.

Whereas a linear time-dependent system of first-order differential equations has only trivial steady-state solutions (all carrier densities zero),[5] nonlinear systems of this kind can have multiple nonzero steady-state solutions given by the equations

$$\Re_i\left(f_{0,1}, f_{0,2}, f_{0,3}, \cdots, f_{0,N}\right) = 0 \ , \qquad i = 1,2,3,\ldots,N \tag{2}$$

In this technical report, 6 types of carriers are considered as listed in Table 1.

Table 1 Densities of carriers in a PL-excited solid-state plasma

Carrier Species	Density Symbols
Electrons	ν_e
Holes	ν_h
e–Trions	τ_e
h–Trions	τ_h
Excitons	n
Photons	φ

3. Reactions

The time dependence of each carrier species is governed by a set of reactions, which defines a path in the phase space of the system that leads to various steady states. Some of these reactions convert one member of a species to a different member of the same species, which can change the temperature of the carrier gas but not its density; this process can act as a kind of "catalysis" that changes other carrier densities while leaving the catalyst's density unchanged.

Let us examine each of the reactions in Sets A–E in detail:

A. Reactions that change the electron density.

Note that Reaction 3 in Table 2 is catalytic as defined above, because it changes the electron and *e*–trion densities without changing the density of excitons. For information on Reaction 4 in this table see Crowne et al.[6] and Blythe and Bloor.[7] The rate equation for electrons is

$$\frac{\partial \nu_e}{\partial t} = G - A\nu_e\nu_h - \frac{1}{2}P\tau_h\nu_e + Y_e n\tau_e + Jn^2 \tag{3}$$

where G is the generation rate due to the incident photon flux from the PL laser, which is fixed.

Table 2 Reactions that change ν_e

Reaction	Rate Constant
1. $\nu_e + \nu_h \rightarrow \varphi$	A
2. $\nu_e + \tau_h \rightarrow$ Ex	P
3. Ex + $\tau_e \rightarrow \nu_e$ + Ex'	Y_e
4. Ex + Ex' $\rightarrow \nu_e + \nu_h$	J

B. Reactions that change the hole density.

Note that Reaction 3 in Table 3 is also catalytic, changing the *h*–trion and hole densities without changing the density of excitons. The rate equation for holes is

$$\frac{\partial \nu_h}{\partial t} = G - A\nu_e\nu_h - \frac{1}{2}N\tau_e\nu_h + Y_h n\tau_h + Jn^2 \tag{4}$$

The factors of $\frac{1}{2}$ appearing in rate Eqs. 3 and 4 serve to "balance" these equations in the chemical sense (i.e., each exciton produced requires 2 parent particles).

Table 3 Reactions that change ν_h

Reaction	Rate Constant
1. $\nu_e + \nu_h \rightarrow \varphi$	A
2. $\nu_h + \tau_e \rightarrow$ Ex	P
3. Ex + $\tau_h \rightarrow \nu_h$ + Ex'	Y_h
4. Ex + Ex' $\rightarrow \nu_e + \nu_h$	J

C. Reactions that change the *e*-trion density.

The third reaction is listed in both Table 2 and Table 4 because it alters the densities of both *e*–trions and excitons, as the rate equation below shows:

$$\frac{\partial \tau_e}{\partial t} = Ln\nu_e - \frac{1}{2}N\tau_e\nu_h - Y_e n\tau_e - K_e\tau_e\tau_h \tag{5}$$

Table 4 Reactions that change τ_e

Reaction	Rate Constant
1. $Ex + \nu_e \rightarrow \tau_e$	L
2. $\nu_h + \tau_e \rightarrow Ex$	N
3. $Ex + \tau_e \rightarrow \nu_e + Ex'$	Y_e
4. $\tau_h + \tau_e \rightarrow Ex$	K_e

D. Reactions that change the *h*–trion density.

Again, the third reaction appears in both Table 3 and Table 5 because it alters the densities of both *h*–trions and excitons, as the rate equation below shows:

$$\frac{\partial \tau_h}{\partial t} = Mn\nu_h - \frac{1}{2}P\tau_h\nu_e - Y_h n\tau_h - K_h\tau_e\tau_h \tag{6}$$

Table 5 Reactions that change τ_h

Reaction	Rate Constant
1. $Ex + \nu_h \rightarrow \tau_h$	M
2. $\nu_e + \tau_h \rightarrow Ex$	P
3. $Ex + \tau_h \rightarrow \nu_h + Ex'$	Y_h
4. $\tau_e + \tau_h \rightarrow Ex$	K_h

E. Reactions that change the exciton density.

The second and third reactions are catalytic agents for the loss of excitons. This implies that the constants *R* and *S* will appear only in the exciton rate equation. The overall rate equation for excitons is

$$\frac{\partial n}{\partial t} = \left\{ \begin{array}{l} Q\nu_e\nu_h - \left(R\nu_e + S\nu_h\right)n - \left(M\nu_h + L\nu_e\right)n \\ +N\tau_e\nu_h + P\tau_h\nu_e + \left(K_e + K_h\right)\tau_e\tau_h - 2Jn^2 \end{array} \right\} \tag{7}$$

Reactions that change *n* are shown in Table 6.

Table 6 Reactions that change n

Reaction	Rate Constant
1. $\nu_e + \nu_h \rightarrow$ Ex	Q
2. Ex + $\nu_e \rightarrow \nu_e$'	R
3. Ex + $\nu_h \rightarrow \nu_h$'	S
4. Ex + $\nu_h \rightarrow \tau_h$	M
5. Ex + $\nu_e \rightarrow \tau_e$	L
6. $\nu_e + \tau_h \rightarrow$ Ex	N
7. $\nu_h + \tau_e \rightarrow$ Ex	P
8. Ex +Ex' $\rightarrow \nu_e + \nu_h$	J
9. $\tau_e + \tau_h \rightarrow$ Ex + Ex'	$K_e + K_h$

4. Charge Neutrality Ansatz

An ansatz that is commonly used in the theory of photoconductivity to solve equations of this kind is local charge neutrality, i.e., particles are created and annihilated in pairs so that there is no accumulation of charge. However, this approach is rigorously correct only for a system with 2 carrier species. An appealing way to generalize it to our case is to assume it applies both to electrons and trions separately, in which case $\nu_e = \nu_h \equiv \nu$ and $\tau_e = \tau_h \equiv \tau$.

Let us consider the full system of 5 equations under the strong-neutrality condition. As a further simplification, let us set the trion–trion constants K_e and K_h to zero. Then the rate-equation system becomes

$$\begin{aligned}
\frac{\partial \nu}{\partial t} &= G - A\nu^2 - \frac{1}{2}P\tau\nu + Y_e n\tau + J \\
\frac{\partial \tau}{\partial t} &= Mn\nu - \frac{1}{2}P\tau\nu - Y_h n\tau \\
\frac{\partial \nu}{\partial t} &= G - A\nu^2 - \frac{1}{2}N\tau\nu + Y_h n\tau + Jn^2 \\
\frac{\partial \tau}{\partial t} &= Ln\nu - \frac{1}{2}N\tau\nu - Y_e n\tau \\
\frac{\partial n}{\partial t} &= \left\{ \begin{array}{l} Q\nu^2 - (R+S+M+N)\nu n \\ +(P+N)\tau\nu - 2Jn^2 \end{array} \right\}
\end{aligned} \tag{8}$$

Because there are 5 equations, this assumption over determines the system. However, it is easily shown that for the special case where $N = P \equiv \Pi$, $L = M \equiv \Lambda$, $Y_e = Y_h \equiv \Upsilon$, and $R = S \equiv \Sigma$, these equations take the form

$$
\begin{aligned}
(9a)\quad & \frac{\partial v}{\partial t} = G - Av^2 - \frac{1}{2}\Pi\tau v + \Upsilon n\tau + Jn^2 \\
(9b)\quad & \frac{\partial \tau}{\partial t} = \Lambda nv - \frac{1}{2}\Pi\tau v - \Upsilon n\tau \\
(9c)\quad & \frac{\partial v}{\partial t} = G - Av^2 - \frac{1}{2}\Pi\tau v + \Upsilon n\tau + Jn^2 \\
(9d)\quad & \frac{\partial \tau}{\partial t} = \Lambda nv - \frac{1}{2}\Pi\tau v - \Upsilon n\tau \\
(9e)\quad & \frac{\partial n}{\partial t} = Qv^2 - 2(\Sigma + \Lambda)vn + 2\Pi\tau v - 2Jn^2
\end{aligned}
\tag{9}
$$

Note that Eqs. 9a and 9c are now identical, as are Eqs. 9b and 9d, respectively. Then in this limit the system size is reduced from 5 to 3 equations and the number of rate constants drops from 10 to 5, so that for this special set of material constants the charge neutrality method yields a valid solution, at least formally.

To find the steady-state densities, we set the time derivatives to zero, which reduces the system (Eq. 9) to the following set of 3 algebraic equations:

$$
\begin{aligned}
(10a)\quad & \frac{1}{2}\Pi v\tau - \Upsilon n\tau = G - Av^2 + Jn^2 \\
(10b)\quad & \frac{1}{2}\Pi v\tau + \Upsilon n\tau = \Lambda nv \\
(10c)\quad & 2(\Sigma + \Lambda)nv + 2\Pi\tau v = Qv^2 - 2Jn^2
\end{aligned}
\tag{10}
$$

By setting $v = xn$ and $\tau = yn$, we obtain the following solutions to Eq. 10:

$$
\begin{aligned}
v_f &= \sqrt{G\left[A + \frac{\Pi - 2\Upsilon x}{\Pi + 2\Upsilon x}\Lambda x - \frac{1}{2}Jx^2\right]^{-1}} \\
n_f &= xv_f \\
\tau_f &= \frac{2\Lambda x}{\Pi + 2\Upsilon x}v_f
\end{aligned}
\tag{11}
$$

where x is a real positive root of the cubic polynomial $4\Lambda\Pi x = \left(Jx^2 + 2\Lambda x - Q\right)(\Pi + 2\Upsilon x)$.

To proceed, we need numbers for the 5 rate constants. To get these constants, we can use the Langevin method[8] (see Appendix), which partitions the recombination into a "hunting" process where the reactants approach each other in real space, followed by an "on-site" event of short duration. Langevin argued that since the contribution of the latter process is small, most of the recombination time comes from the "hunting" phase. We will argue that that this scenario is appropriate for recombination kinetics in TMDs for the following reasons:

1) The large binding energy of excitons and other many-body complexes in TMDs suggests that they are compact in real space (i.e., Frenkel-like objects) with large effective masses and hence low mobilities, a characteristic that is enhanced by strong electron–phonon coupling, poor material quality, etc.

2) The *d*–state nature of the conduction and valence bands of TMDs implies that for such complexes recombination takes place between atomic states. This implies that the matrix elements for atomic-level decay processes are large, and hence the "on-site" recombination time is small.

Interaction between pairs of complexes is governed by the electrostatic forces between them. Although the interaction mechanism for recombination is strictly quadratic in this technical report, Table 7 lists the various force laws that mediate these interactions and enter into Langevin's theory. We will treat excitons as neutral polarizable entities whose interactions with charge carriers and trions resemble those of nonpolar molecules.

Table 7 Force laws that mediate Langevin recombination between carrier species: $\mu_{e,h}$—electron/hole mobilities, μ_{tr}—trion mobilities, and μ_{ex}—exciton mobilities.

Recombining Pair	Rate Constant	Force Law	Langevin Coefficient
1. Ex, ν Nonpolar dipole + charge	Λ, Σ	r^{-5}	$\frac{q}{\varepsilon\varepsilon_0}\left(\mu_{ex}+\mu_{e,h}\right)$
2. ν, τ Charge + charge	Π	r^{-2}	$\frac{q}{\varepsilon\varepsilon_0}\left(\mu_{e,h}+\mu_{tr}\right)$
3. Ex, τ Nonpolar dipole + charge	ϒ	r^{-5}	$\frac{q}{\varepsilon\varepsilon_0}\left(\mu_{ex}+\mu_{tr}\right)$
4. τ, τ Charge + charge	K	r^{-2}	$\frac{q}{\varepsilon\varepsilon_0}\left(\mu_{tr}+\mu_{tr}\right)$
5. Ex, Ex Nonpolar dipole + Nonpolar dipole	*J*	r^{-7}	London dispersive force

5. Experimental Orders of Magnitude for Rate Constants

In order to test the relevance of these calculations, we can estimate the densities of the various carrier species predicted by this theory within a 2-D, PL-excited MoS_2 monolayer. In our steady-state experiments,[9] we used a 532-nm laser (photon energy 2.33 eV) to create an incident intensity of 140 $\mu W/\mu m^2$ at the sample surface, which corresponds to a photon flux of

$\sim 3.75 \times 10^{22}$ photons/$\left(\text{cm}^2 \cdot \text{s}\right)$. A quantum yield for electron-hole pair creation of 0.004 would create a generation flux G within the monolayer of $\sim 1.5 \times 10^{20}$ eh pairs/$\left(\text{cm}^2 \cdot \text{s}\right)$. Assuming that the Langevin approach is appropriate, we can use our in-house samples of 2-D MoS_2 with field-effect transistor mobilities μ = 10 $\text{cm}^2/\left(\text{V-s}\right)$ to derive $\alpha = \mu q / \left(\varepsilon \varepsilon_0\right) = 1.8 \times 10^{-5}\,\text{cm}^3/\text{s}$ and

$A = 4\pi\alpha = 2.3 \times 10^{-4}\,\text{cm}^3/\text{s}$. If only the *A*-type recombination process operated, this value in tandem with *G* would predict an equivalent steady-state carrier density $n_{e,h} = \sqrt{\frac{G}{A}} = 8.07 \times 10^{11}\ \text{cm}^{-3}$.

6. Numerical Simulation

By restoring the time derivatives to the truncated version of Eq. 9, we obtain a system of 3 ordinary differential equations that is amenable to solution by numerical simulation, notably by using the routine NDSolve in the *Mathematica* package. Let us assume that all of the rate constants are the same order of magnitude, as listed in Table 8.

Table 8 Rate constants for Eq. 2

Rate Constant	Value
Π	$4. \times 10^{-4}$
Λ	$4. \times 10^{-6}$
Υ	$1. \times 10^{-5}$
J	$1. \times 10^{-4}$
Q	$1. \times 10^{-5}$

Restoring the time derivatives results in the time-dependent system

$$\begin{aligned} (12a) \quad & \frac{\partial v}{\partial t} = G - Av^2 - \frac{1}{2}\Pi\tau v + \Upsilon n\tau + \frac{1}{2}Jn^2 \\ (12b) \quad & \frac{\partial \tau}{\partial t} = \Lambda n v - \frac{1}{2}\Pi\tau v - \Upsilon n\tau \\ (12c) \quad & \frac{\partial n}{\partial t} = Qv^2 - 2\Lambda v n + 2\Pi\tau v - Jn^2 \end{aligned} \tag{12}$$

with the same fixed-point solutions as Eq. 11:

$$
\begin{aligned}
v_f &= \sqrt{G\left[A + \frac{\Pi - 2\Upsilon x}{\Pi + 2\Upsilon x}\Lambda x - \frac{1}{2}Jx^2\right]^{-1}} \\
n_f &= xv_f \\
\tau_f &= \frac{2\Lambda x}{\Pi + 2\Upsilon x} v_f
\end{aligned}
\tag{13}
$$

where x is again a real positive root of cubic polynomial $4\Lambda\Pi x = \left(Jx^2 + 2\Lambda x - Q\right)\left(\Pi + 2\Upsilon x\right)$. In principle as many as 3 steady states are therefore possible. Using the experimental numbers $G = 1.5\times10^{20}$ eh pairs/$\left(\text{cm}^2 \cdot \text{s}\right)$, $\Lambda = 2.5\times10^{-3}$, and $A = 2.3\times10^{-4}\,\text{cm}^3/\text{s}$ together with the rate constants listed in Table 8, we find that there is one real root for the cubic, which gives

$$
\begin{aligned}
v_f &= 8.16\times10^{11}\ \text{cm}^{-3} \\
n_f &= 8.49\times10^{10}\ \text{cm}^{-3} \\
\tau_f &= 1.69\times10^{9}\ \text{cm}^{-3}
\end{aligned}
\tag{14}
$$

For these values of the various rate constants, in steady state the majority of the carriers are *eh* pairs, followed by excitons and then by trions. Running the time simulation by switching on the laser at t = 0 with starting values $v(t=0) = n(t=0) = \tau(t=0) = 0$ gives the plot shown in Fig. 1:

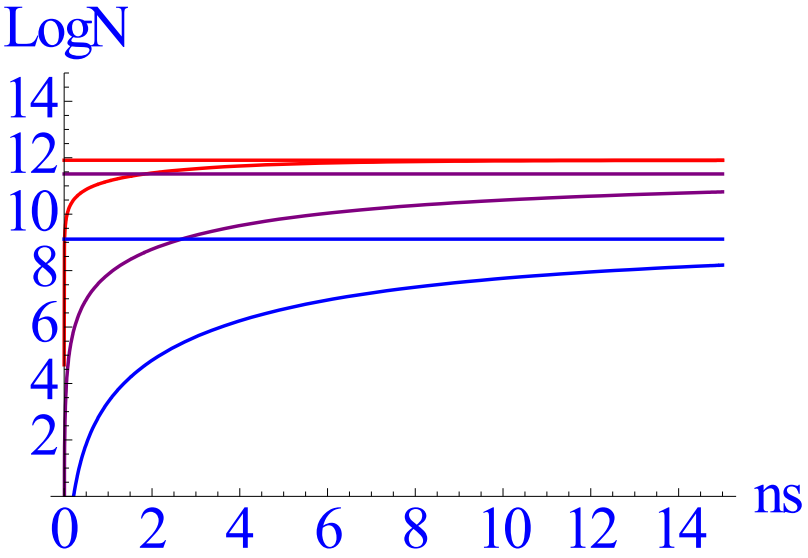

Fig. 1 Time dependence of carrier species for $\Lambda = 4.\times10^{-6}$. Red—electron-hole pairs, magenta—excitons, and blue—trions.

Note that the fastest rise time is for the *eh* pairs, followed by excitons and then by trions.

It is also noteworthy that the constant Λ, which converts an exciton into a trion, is very small. Suppose we increase it to 2.5×10^{-4}. The new simulation results shown in Fig. 2 exhibit several new features. First of all, the fixed point has moved:

$$\begin{aligned} \nu_f &= 8.16\times10^{11}\ \text{cm}^{-3} \\ n_f &= 3.99\times10^{12}\ \text{cm}^{-3} \\ \tau_f &= 6.41\times10^{12}\ \text{cm}^{-3} \end{aligned} \tag{15}$$

and now predicts that there are now more trions than excitons. In addition, the simulation now shows changes in the transient behavior:

1) The *eh* density seems to saturate around 10 ns, but then develops a minimum in the range from 10 ns to 140 ns before reaching a true steady state.

2) Initially there are more excitons than trions, with a crossover around 20 ns. The exciton curve is nearly linear over a wide range from 10 ns to 50 ns.

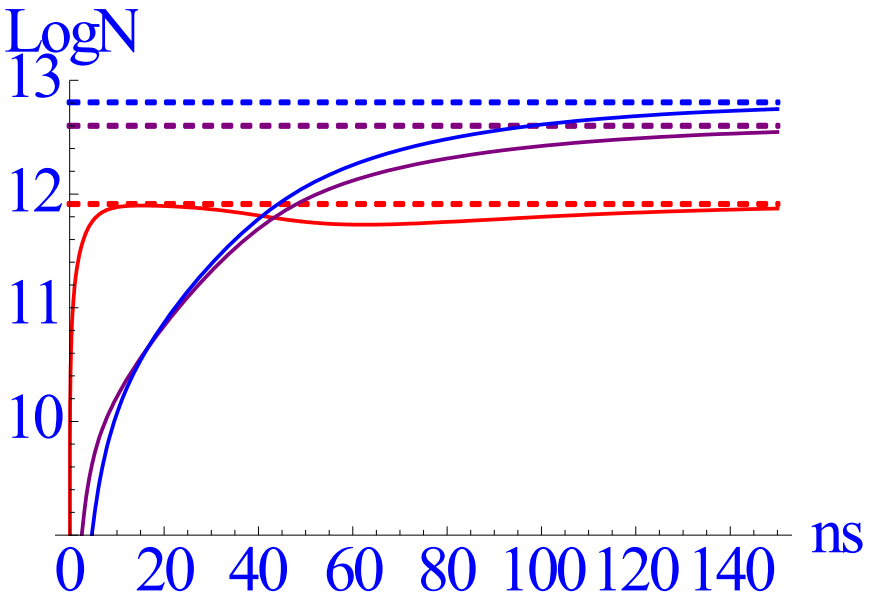

Fig. 2 Time dependence of carrier species for Λ = 4. × 10^{-4}. Red—electron-hole pairs, magenta—excitons, and blue—trions.

These features are more pronounced when $\Lambda = 2.5\times10^{-3}$, for which the new fixed point is at

$$
\begin{aligned}
\nu_f &= 8.16\times10^{11}\ \mathrm{cm}^{-3} \\
n_f &= 1.15\times10^{13}\ \mathrm{cm}^{-3} \\
\tau_f &= 1.35\times10^{14}\ \mathrm{cm}^{-3}
\end{aligned}
\tag{16}
$$

Next, Fig. 3 graphically exhibits the time dependence of carrier species for $\Lambda = 4. \times 10^{-3}$.

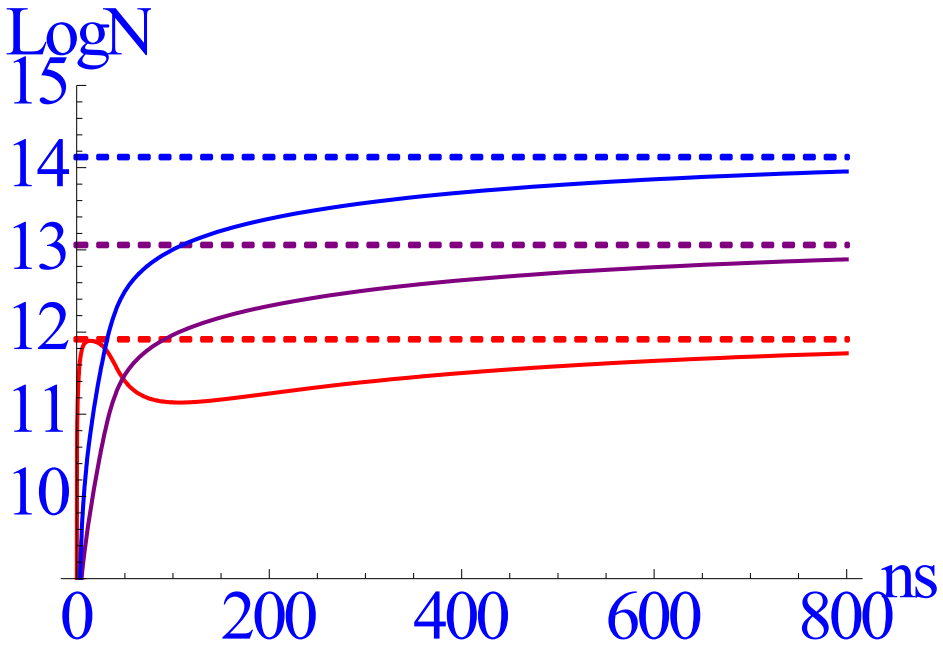

Fig. 3 Time dependence of carrier species for $\Lambda = 4. \times 10^{-3}$. Red—electron-hole pairs, magenta—excitons, and blue—trions.

Another parameter of interest is *J*, which controls the decay of excitons into *eh* pairs by exciton–exciton collisions. This reaction is complementary to the parameter *A*, which mediates the creation of excitons from photons. For the simulation plotted in Fig. 1, *J* was set to 1.0×10^{-4}; decreasing *J* to 1.0×10^{-6} results in a new fixed point and the transient behavior shown in Fig. 4:

$$
\begin{aligned}
\nu_f &= 8.16\times10^{11}\ \mathrm{cm}^{-3} \\
n_f &= 4.89\times10^{12}\ \mathrm{cm}^{-3} \\
\tau_f &= 7.52\times10^{10}\ \mathrm{cm}^{-3}
\end{aligned}
\tag{17}
$$

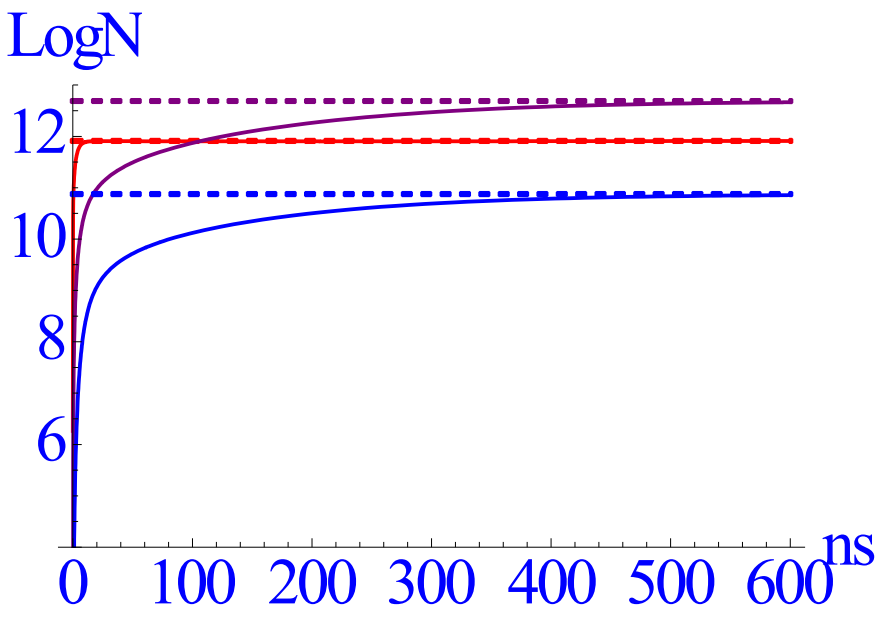

Fig. 4 Time dependence of carrier species for $J = 4. \times 10^{-6}$. Red—electron-hole pairs, magenta—excitons, and blue—trions.

Decreasing J results in a rapid rise time and saturation for the *eh* pairs, while excitons and trions increase more slowly, with the former saturating above the *eh* pairs and the latter below them. Increasing J to 1.0×10^{-3} results in the fixed point

$$\begin{aligned} v_f &= 8.16 \times 10^{11}\ \text{cm}^{-3} \\ n_f &= 8.49 \times 10^{10}\ \text{cm}^{-3} \\ \tau_f &= 1.69 \times 10^{9}\ \text{cm}^{-3} \end{aligned} \tag{18}$$

and the time history shown in Fig. 5. Now all of the carrier densities rise and saturate rapidly, with the trion population the smallest and eh pair population the largest.

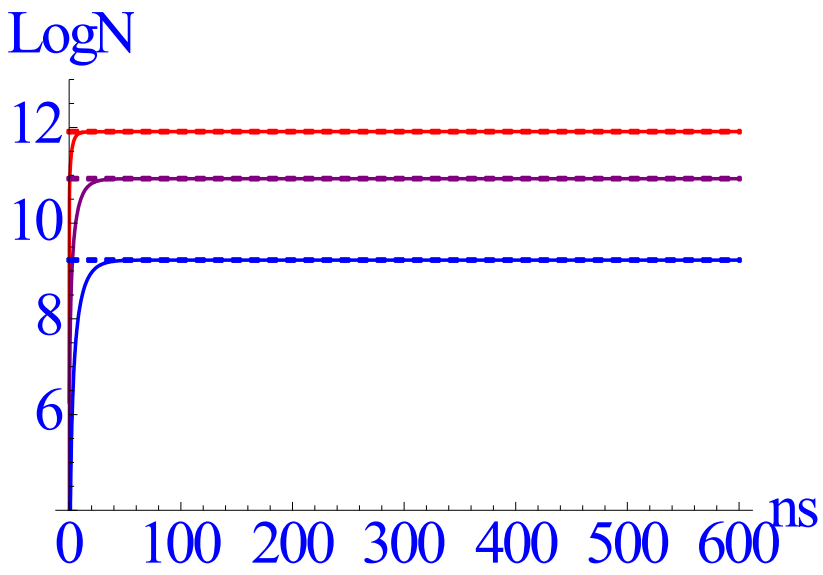

Fig. 5 Time dependence of carrier species for $J = 4. \times 10^{-3}$. Red—electron-hole pairs, magenta—excitons, and blue—trions.

The final parameter of interest is Q, which controls the creation of excitons by electron–hole collisions. It is noteworthy that all the simulation results presented up to now have predicted the same steady-state *eh* pair density, i.e., 8.16×10^{11} cm^{-3}, regardless of how the other reaction constants are varied. To investigate this behavior, let us use the system (Eq. 8) to construct the quantity $2\frac{\partial v}{\partial t} + 2\frac{\partial \tau}{\partial t} + \frac{\partial n}{\partial t}$. This leads to a detailed-balance type of equation of the form

$$2\frac{\partial v}{\partial t} + 2\frac{\partial \tau}{\partial t} + \frac{\partial n}{\partial t} = 2G - (2A - Q)v^2 \tag{19}$$

If we postulate that the system *has* a steady state, we can state that the combination of derivatives $2\frac{\partial v}{\partial t} + 2\frac{\partial \tau}{\partial t} + \frac{\partial n}{\partial t} = 0$; then (19) implies the relation $v = \sqrt{\frac{2G}{2A - Q}}$. For the constants we have chosen, this gives 8.16×10^{11} cm^{-3}, i.e., in exact agreement with the value of v predicted by the simulations. This result would be useful except that the argument is actually circular, in the sense that if we consider the case where $Q > 2A$, the system clearly does *not* have a steady state. In fact, as shown in Fig. 6, the response predicted by simulation is "explosive", and the simulation program responds to this state of affairs by terminating at a time of approximately 60 ns, beyond which it cannot solve the problem.

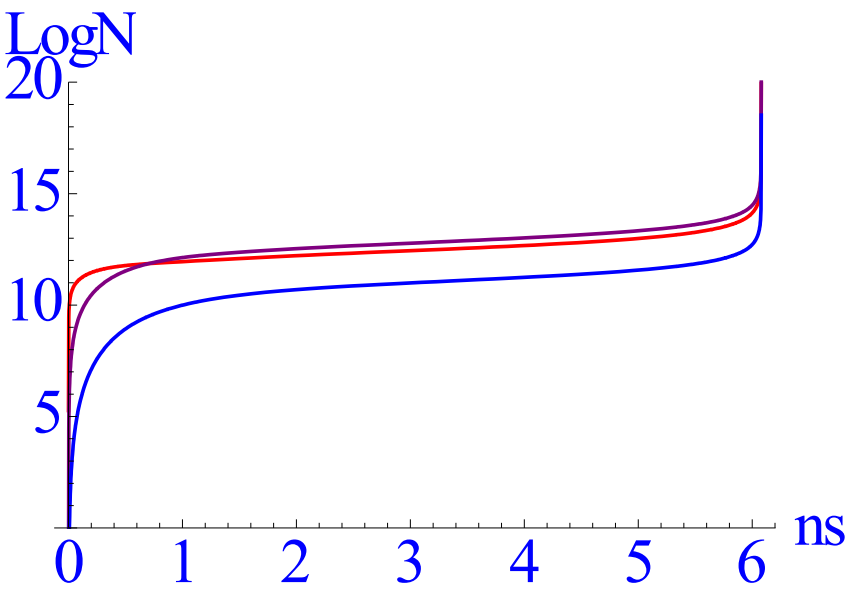

Fig. 6 Explosive behavior of simulation with Q > 2A. System (Eq. 8) has no steady state, forcing the simulation program to terminate at a time of approximately 60 ns.

7. Strong vs. Weak Neutrality

On the surface, the assumption of equal densities should be a reasonable starting point for analysis of the carrier dynamics. However, since the correct problem involves 5 rate equations, there are 2 ways to implement charge neutrality: the ansatz of Section 4 above, which we will refer to as "strong charge neutrality", and also a "weak charge neutrality" condition, for which $\nu_e + \tau_e = \nu_h + \tau_h$. This approximation reduces the number of equations from 5 to 4. Which is the right choice?

One way to test the validity of the strong-neutrality condition is to check for stability of the system when this condition is weakly violated. For this we use the full 5-equation system with the special set of coefficients but allowing all 5-carrier densities to be unequal, which reads

$$\begin{aligned}
\frac{\partial \nu_e}{\partial t} &= G - A\nu_e\nu_h - \frac{1}{2}\Pi\tau_h\nu_e + \Upsilon n\tau_e + Jn^2 \\
\frac{\partial \nu_h}{\partial t} &= G - A\nu_e\nu_h - \frac{1}{2}\Pi\tau_e\nu_h + \Upsilon n\tau_h + Jn^2 \\
\frac{\partial \tau_e}{\partial t} &= \Lambda n\nu_e - \frac{1}{2}\Pi\tau_e\nu_h - \Upsilon n\tau_e \\
\frac{\partial \tau_h}{\partial t} &= \Lambda n\nu_h - \frac{1}{2}\Pi\tau_h\nu_e - \Upsilon n\tau_h \\
\frac{\partial n}{\partial t} &= Q\nu_e\nu_h - 2\Lambda\left(\nu_e + \nu_h\right)n + \Pi\left(\tau_e\nu_h + \tau_h\nu_e\right) - 2Jn^2
\end{aligned} \tag{20}$$

The steady-state solution to this system satisfies the strong-neutrality condition; let us perturb the densities around this solution as follows:

$$\begin{aligned} \nu_e &= \nu + \delta\nu_e \\ \nu_h &= \nu + \delta\nu_h \\ \tau_e &= \tau + \delta\tau_e \\ \tau_h &= \tau + \delta\tau_h \\ n &= n_0 + \delta n \end{aligned} \tag{21}$$

This leads to the linear perturbation equation

$$\frac{\partial}{\partial t}\begin{pmatrix} \delta\nu_e \\ \delta\nu_h \\ \delta\tau_e \\ \delta\tau_h \\ \delta n \end{pmatrix} = \mathsf{M}\begin{pmatrix} \delta\nu_e \\ \delta\nu_h \\ \delta\tau_e \\ \delta\tau_h \\ \delta n \end{pmatrix} \tag{22}$$

with

$$\mathsf{M} = \begin{pmatrix} -\left(A\nu + \frac{1}{2}\Pi\tau\right) & -(A\nu) & \Upsilon n_0 & -\left(\frac{1}{2}\Pi\nu\right) & \Upsilon\tau + 2Jn_0 \\ -(A\nu) & -\left(A\nu + \frac{1}{2}\Pi\tau\right) & -\left(\frac{1}{2}\Pi\nu\right) & \Upsilon n_0 & \Upsilon\tau + 2Jn_0 \\ \Lambda n_0 & -\left(\frac{1}{2}\Pi\tau\right) & -\left(\frac{1}{2}\Pi\nu + \Upsilon n_0\right) & 0 & \Lambda\nu - \Upsilon\tau \\ -\left(\frac{1}{2}\Pi\tau\right) & \Lambda n_0 & 0 & -\left(\frac{1}{2}\Pi\nu + \Upsilon n_0\right) & \Lambda\nu - \Upsilon\tau \\ Q\nu - 2\Lambda n_0 + \Pi\tau & Q\nu - 2\Lambda n_0 + \Pi\tau & \Pi\nu & \Pi\nu & -4\left(Jn_0 + \Lambda\nu\right) \end{pmatrix} \tag{23}$$

The stability criterion is that the eigenvalues of this equation all have negative real parts; this ensures that any departure from the fixed point will decay back to it. Using the first set of rate constants and the corresponding fixed point of the equations

$$\begin{aligned} \nu_f &= 8.16\times10^{11}\ \text{cm}^{-3} \\ n_f &= 8.49\times10^{10}\ \text{cm}^{-3} \\ \tau_f &= 1.69\times10^{9}\ \text{cm}^{-3} \end{aligned} \tag{24}$$

the eigenvalues λ_I are easily evaluated numerically:

$$\begin{aligned}\lambda_1 &= -3.81\times10^{8}\\ \lambda_2 &= -1.79\times10^{8}\\ \lambda_3 &= -1.68\times10^{8}\\ \lambda_4 &= -1.13\times10^{8}\\ \lambda_5 &= +1.15\times10^{6}\end{aligned} \tag{25}$$

The sign of λ_5 reveals that in fact the solution to the system with strong neutrality is not a fixed point of the system, from which we may conclude that the true system has a steady state with weak neutrality (i.e., the SSP has more electrons than holes and more *h*–trions than *e*–trions to compensate it).

8. Conclusions

The analysis given here only scratches the surface of this problem, both mathematically and with regard to the physics of transport in 2-D systems. Use of Langevin's formula should clearly be a point of contention; the work of Juška et al.[10] on low-mobility layered systems for solar cells indicate that the dimensionality of the system enters strongly, converting the simple bimolecular law in 3-D to a 2-D expression involving fractional powers of the densities. In addition, Greenham and Bobbert[11] have observed that the transport is partially diffusive; that is, the Langevin dependence takes into account only the drift of the particles in a Coulomb field. Finally, it is possible to take some temperature dependence into account by introducing the "Coulomb radius" $r_C = q^2 / 4\pi\varepsilon\varepsilon_0 kT$ as a boundary between Langevin's carrier approach and the "black hole" where the carriers recombine. We plan to discuss these matters in a future publication.

9. References

1. Haug A. Theoretical solid state physics. Vol. 2. Oxford (NY): Pergamon Press; 1972. Chapter V.C.
2. Nelson DB, Nelson KA. Coherent measurements of high-order electronic correlations in quantum wells. Nature. 2010;466:1089–1092.
3. Mak KF, He K, Lee CG, Lee GH, Hone J, Heinz TF, Shan J. Tightly bound trions in monolayer MoS_2. Nat Mater. 2013;126:207–211.
4. Yariv A. Quantum electronics. 3rd ed. New York: Wiley & Sons; 1987. p. 192.
5. Minorsky N. Introduction to non-linear mechanics: Topological methods, analytical methods, non-linear resonance, relaxation oscillations. Ann Arbor (MI): J.W. Edwards; 1947. Part 1, ch. 1.
6. Crowne FJ, Amani M, Birdwell AG, Chin ML, O'Regan TP, Najmaei S, Liu Z, Ajayan PM, Lou J, Dubey M. Blueshift of the A-exciton peak in folded monolayer 1H MoS2. Phys Rev B. 2013;88:235302.
7. Blythe R, Bloor D. Electrical properties of polymers. 2nd ed. New York: Cambridge University Press; 2005. p. 299.
8. Langevin P. Ann Chim Phys. 1903;28:433.
9. Lanzillo NA, Birdwell AG, Amani M, Crowne FJ, Shah PB, Najmaei S. Temperature-dependent phonon shifts in monolayer MoS_2. Appl Phys Lett. 2013;103:093102.
10. Juška G, Genevičius K, Nekrašas N, Sliaužys G, Österbacka R. Two dimensional Langevin recombination in regioregular poly(3-hexylthiophene). Appl Phys Lett. 2009;95:013303.
11. Pivrikas A, Juška G, Österbacka R, Westerling M, Viliunas M, Arlauskas K, Stubb H. Langevin recombination and space-charge-perturbed current transients in regiorandom poly(3-hexylthiophene). Phys Rev B. 2005;71:125205.
12. Greenham NC, Bobbert PA. Two-dimensional electron-hole capture in a disordered hopping system, Phys Rev B. 2003;68:245301.
13. Schiff LI. Quantum mechanics. 2nd ed. New York: McGraw-Hill; 1955. p. 180.

List of Symbols, Abbreviations, and Acronyms

MoS_2	molybdenum disulfide (a TMD)
PL	photoluminescence
SSP	solid-state plasma
TMD	transition-metal dichalcogenide
2-D	2-dimensional
3-D	3-dimensional

1 DEFENSE TECHNICAL
(PDF) INFORMATION CTR
DTIC OCA

2 DIRECTOR
(PDF) US ARMY RSRCH LAB
RDRL CIO LL
IMAL HRA MAIL & RECORDS MGMT

1 GOVT PRINTG OFC
(PDF) A MALHOTRA

42 US ARMY RSRCH LAB
(HCS) ATTN RDRL SER P AMIRTHARAJ
ATTN RDRL SED E D KATSIS
ATTN RDRL SED E K A JONES
ATTN RDRL SEE I S SVENSSON
ATTN RDRL SEE I W BECK
ATTN RDRL SEE I K K CHOI
ATTN RDRL SEE I V PARAMESHWARAN
ATTN RDRL SEE I M REED
ATTN RDRL SEE I W M GOLDING
ATTN RDRL SER E E VIVEIROS
ATTN RDRL SER E L. DE LA CRUZ
ATTN RDRL SER E E FORSYTHE
ATTN RDRL SER E K MCKNIGHT
ATTN RDRL SER E D MORTON
ATTN RDRL SER E J PENN
ATTN RDRL SER E D A RUZMETOV
ATTN RDRL SER E P SHAH
ATTN RDRL SER E J QIU
ATTN RDRL SER E J WILSON
ATTN RDRL SER E J WEIL
ATTN RDRL SER E K F TOM
ATTN RDRL SER E F CROWNE (10 HC)
ATTN RDRL SER E G BIRDWELL
ATTN RDRL SER E R DEL ROSARIO
ATTN RDRL SER E T IVANOV
ATTN RDRL SER L B H PIEKARSKI
ATTN RDRL SER L B NICHOLS
ATTN RDRL SER L M CHIN
ATTN RDRL SER L R A BURKE
ATTN RDRL SER L M DUBEY
ATTN RDRL SER L S NAJMAEI
ATTN RDRL SER L M ERVIN
ATTN RDRL SER L R POLCAWICH

INTENTIONALLY LEFT BLANK.